Journal of Alloys and Compounds 509 (2011) 6522–6527

Contents lists available at ScienceDirect

Journal of Alloys and Compounds

journal homepage: www.elsevier.com/locate/jallcom

Phase transformation and exchange bias effects in mechanically alloyed Fe/magnetite powders

O. Crisan*, A.D. Crisan

National Institute for Materials Physics, P.O. Box MG-7, 077125 Bucharest-Magurele, Romania

ARTICLE INFO

Article history:
Received 3 March 2009
Received in revised form 25 March 2011
Accepted 28 March 2011
Available online 5 April 2011

PACS:
75.50.−y
75.50.Tt
81.20.Ev
61.10.N

Keywords:
Ferromagnet/antiferromagnet systems
Nanograin powders
Structural phase transformation
Exchange bias effect

ABSTRACT

Nanostructured powders processed by ball milling of a mixture of Fe and Fe_3O_4 at room temperature are shown to undergo an incomplete redox reaction with formation of FeO during the milling process. This reaction is favored by the high energy introduced during the mechano-alloying process. Concurrent effects of milling such as grain refinement down to the nanometre scale lead at the end of the milling processes to a mixed multiphase powder of nanograins, with Fe and Fe oxide grains inter-dispersed. We show that in the as-milled Fe/Fe_3O_4 powder, during milling process, wüstite (FeO) is formed as a consequence of the redox reaction. Moreover, with increasing temperature, the system undergoes an inverse phase transformation towards the initial Fe and Fe_3O_4 phases until about 450 °C. Above this temperature the reduction reaction Fe + Fe_3O_4 = 4FeO is reinitiated, resulting in sharp decrease of Fe and Fe_3O_4 content from about 550 °C and almost complete disappearance of these phases at about 900 °C. This transformation was investigated via an energy-dispersive in situ X-ray diffraction experiment using the synchrotron radiation. This study allows direct collection of X-ray patterns after few minutes exposure, at selected temperatures, ranging between 20 °C and 1000 °C. The structural and magnetic characterizations of the nanograin powders, as-milled and annealed at several temperatures, are studied using XRD, SEM and magnetic measurements. Such ferromagnetic–antiferromagnetic composites are extensively studied as they exhibit exchange bias effect, with a large impact in technological applications. The magnetic behaviour and intrinsic mechanisms leading to the occurrence of exchange bias effects are discussed and related to the samples microstructural features. A significant exchange bias effect, related to FeO content, is observed for as-milled sample, the effect being less pronounced upon annealing the nanograin powder.

1. Introduction

Granular systems of Fe nanoparticles embedded in iron oxide matrix have attracted a great deal of interest due to the observed magnetic exchange bias effect in such systems [1–3]. The exchange bias effect, defined as the shift of the hysteresis loop in ferromagnetic (FM)–antiferromagnetic (AFM) systems upon cooling down below the Néel temperature of the AFM phase [4,5], has been shown to occur in granular ball-milled Fe/Fe oxide powders [1,2]. It usually arises due to the coupling between FM and AFM grains at the interfaces, but has been revealed also in systems containing ferrimagnetic (FI) phases and disordered phases with spin-glass behaviour [3]. Therefore, the degree of structural disorder induced by the ball milling and the nanograin size distributions within the granular mixed FM/AFM powders are key factors for the exchange bias in granular systems. Mechanically alloyed mixtures of Fe and magnetite (Fe_3O_4) [6], and Fe and hematite (Fe_2O_3) [7] were shown to result in formation of wüstite (FeO) via a chemical reduction reaction occurring during the ball milling. Upon annealing FeO may decompose into the constituent powders [6]. The evolution of phase composition in such mixtures has a strong influence on the magnetic properties and the exchange bias effect, in particular and therefore needs to be strictly controlled during annealing, if the granular systems are to be used for technological applications.

We have processed a non-equimolar mixture of iron and magnetite by ball milling and we have studied the phase transformation that occurs during dynamic annealing in such systems via a unique tool of in situ characterization: temperature dependent X-ray diffraction of synchrotron radiation. Magnetic behaviour of as-milled and annealed samples are presented and interpreted in correlation with the phase composition in the samples.

2. Experimental

The Fe/Fe_3O_4 mixed powder (2:8 mass%) has been prepared by ball milling in a Retzsch PM 400 planetary ball mill with 4 vials. The total amount of the sample was 10 g, and the powders used were of high purity (99.99+%). The experimental con-

* Corresponding author.
E-mail address: ocrisan@yahoo.com (O. Crisan).

0925-8388/$ – see front matter © 2011 Elsevier B.V. All rights reserved.
doi:10.1016/j.jallcom.2011.03.147

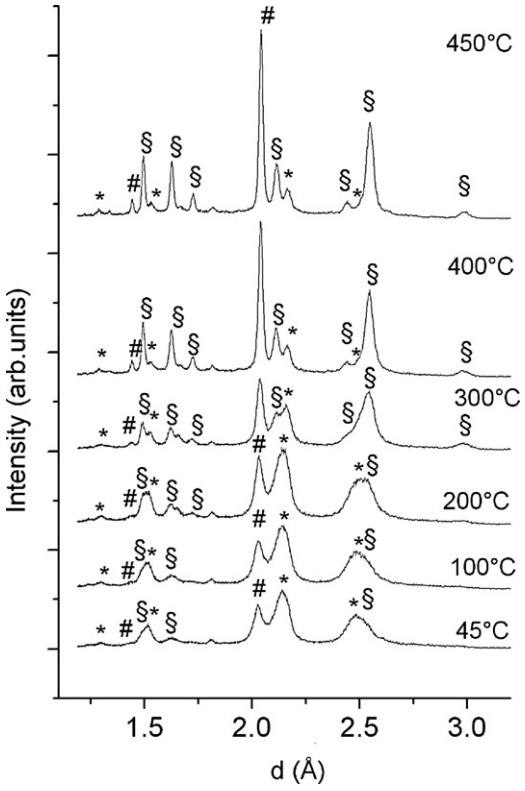

Fig. 1. XRD patterns taken at selected temperatures between 45 °C and 450 °C. The following phases are indexed on figure: # – α-Fe, * – FeO and § – Fe_3O_4. The patterns are given in units of reticular distances.

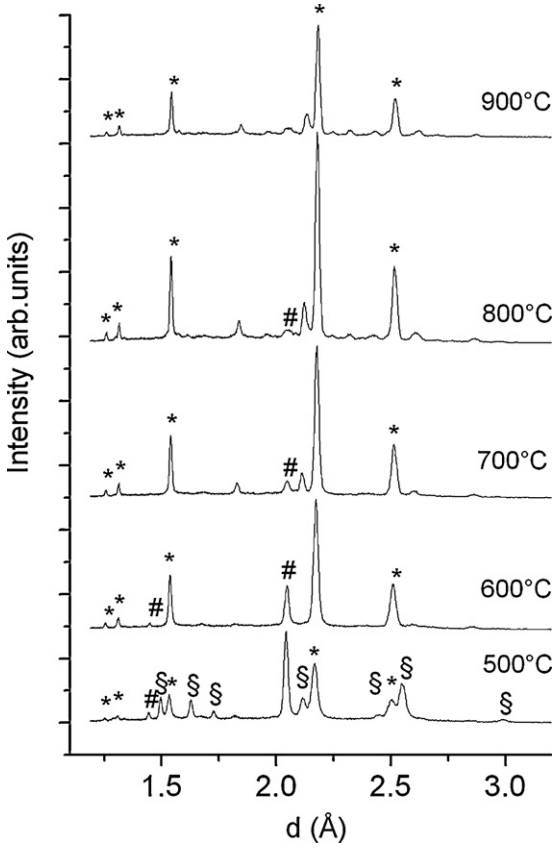

Fig. 2. XRD patterns taken at selected temperatures between 500 °C and 900 °C. The following phases are indexed on figure: # – α-Fe, * – FeO and § – Fe_3O_4. The patterns are given in units of reticular distances.

ditions were: sun wheel frequency 200 rpm, sun wheel/vial frequency ratio 1.5, the loading constant 8; ball size 20 mm, ball-to-powder mass ratio 1/40 and number of tungsten carbide balls used was 8. The powder and balls were sealed together with hexane as protective media, against uncontrolled oxidation. Total milling time was 50 h. The energy-dispersive in situ synchrotron X-ray diffraction [8] study was done at DESY-HASYLAB Hamburg at Max 80 F2.1 beamline, dedicated to the diffraction studies of materials under extreme conditions (high temperature/high pressure). The diffraction patterns are recorded in grazing incidence with step-scanning mode single runs using synchrotron radiation wavelength of 1.2 Å. The energy range covered by the high-purity Ge solid-state detector is between 2 keV and 80 keV. Pure NaCl mounted in the sample boron cube was used for energy calibration and the resulting diffraction patterns are therefore given directly in units of reticular distance, for simplicity. The temperature was controlled by a PtRh thermocouple placed inside the cube and the sample was heated in steps of 20 °C. Each pattern is collected using an average exposure of 2 min.

Parts of as-milled powders have been isothermally annealed in a high vacuum chamber, with a base pressure better than 10^{-5} mbar using a temperature-controlled heating cell. Annealings were done at 250 °C, 400 °C, 550 °C and 720 °C for 1 h. Scanning electron microscopy (SEM) images were obtained using a Carl Zeiss Supra 40 VP FEG. Magnetic measurements have been performed using a vibrating sample magnetometer (VSM) in a temperature range between 4.2 K and 300 K. The hysteresis loops were recorded as follows: (i) cooling to 4.2 K without the presence of external field and first loop (ZFC at 4.2 K) was measured; (ii) heated up and recording the loop at 280 K; (iii) again, cooling to 4.2 K in 5 T applied field (FC) and the loop was measured.

3. Results and discussion:

3.1. Structural phase transformation

In Fig. 1 we present the synchrotron XRD patterns taken at several, selected temperatures, from 45 °C to 450 °C. The pattern at 45 °C presents broad peaks, typical for nanostructured materials. We are able to identify the main Bragg reflections of the α-Fe, FeO (wüstite) and Fe_3O_4 (magnetite). As the initial mixed powders were α-Fe and Fe_3O_4 the observation of the Bragg reflections of the wüstite is the proof of an un-complete redox reaction that develops during the milling, in agreement with previous results [4]. We are interested in following the evolution of the phase structure with the temperature. With increasing the temperature, as expected, the Bragg reflections continuously narrow due to the coarsening of the structure by grain growth and agglomeration of the grains. The observed sharpening of the peaks is nevertheless related also to the decrease of the lattice microstrains, as the temperature is increased, an issue that will be addressed below. We observe the gradual decrease of the relative intensity of the main Bragg peak of the wüstite, with increasing the temperature up to around 450 °C. In the mean time, the relative contents of the other constituent phases, α-Fe and Fe_3O_4, are more or less the same. It seems that the redox reaction that formed the FeO phase is reversible and with increasing temperature, iron and magnetite become the predominant phases.

At 450 °C the main reflection of the wüstite is only about 12% of the main diffraction peak of the iron. But, at around 500 °C (Fig. 2), upon further increase of the temperature, the wüstite phase starts to form again, its main Bragg peak, increasing to about 63% of the iron peak. The new reduction of the magnetite to wüstite occurs quite fast, therefore at 600 °C, the diffraction pattern sees no more magnetite peaks, but only FeO and α-Fe Bragg reflections, with FeO becoming the dominant phase.

The oxidation of the iron continues with increasing temperature. At 900 °C the iron main diffraction peak represents only about 6% of the main FeO (2 0 0) Bragg reflection: After around 1000 °C the samples starts to melt, as seen by the extreme broad diffraction pattern, not shown here. By cooling the sample after the end of the measurement we observe that the oxidation is irreversible, the pattern of the quenched sample exhibits only the Bragg peaks of the FeO phase.

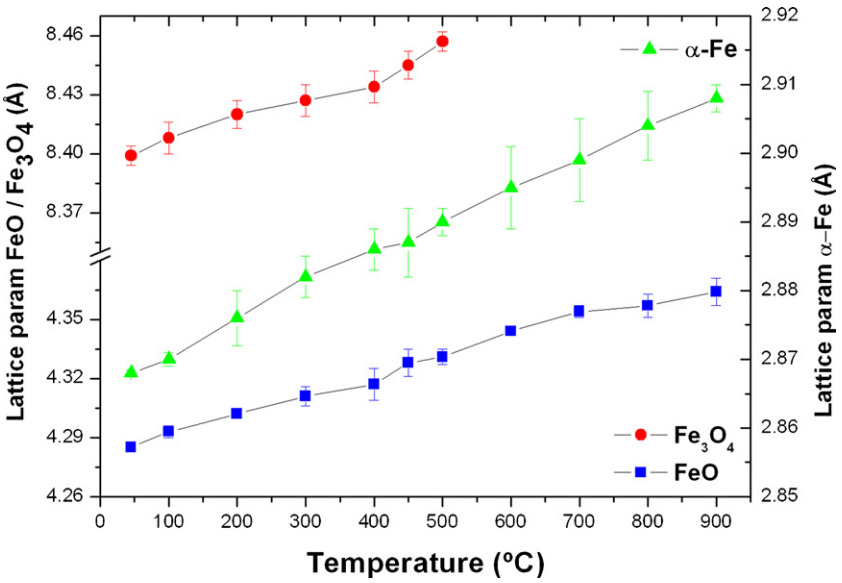

Fig. 3. Temperature evolution of lattice parameters of the identified phases.

We have applied full-profile refinement procedure on the XRD patterns in order to obtain with accuracy the phase composition as well as structural parameters such as: lattice parameters, unit cell volume, average grain sizes and lattice microstrains using the integral breadth method as well as the possible crystallographic texture. Our patterns show large overlapped Bragg peaks, especially at low temperatures. In intermetallic alloys such large patterns are characteristic of materials with small nano-crystals [9–11] with structural disorder [12,13] or predominant amorphous-like structure [14]. Therefore, in order to correctly deconvolute and assign the observed peaks, a refinement fitting procedure had to be performed. All the patterns have been fitted using Datlab program [15]. This powder diffraction package, developed for polycrystalline multiple phase materials, allows deconvolution of complex overlapping Bragg peaks, calculation of position and line-width of each individual Bragg reflection and the determination of lattice parameters. The Bragg peaks of the diagrams have been fitted to a pseudo-Voigt line profile. The Voigt profile is a spectral line that can account for peak broadening by two mechanisms. The first one is strain-related and would produce a Gaussian profile, and the other is related to the size of the grains and would produce a Lorentzian profile. By using the lattice parameters, line-widths and mixing parameters obtained for each Bragg reflection, we were able to calculate the average crystallographic domain size associated with the average diameter of the grains. The method we used is based on the integral breadth algorithm. The integral breadth β is defined as the peak area divided by the maximum height of the peak. The integral-breadth method summarized in [16] calculates the root-mean-square strain (RMSS) and both surface- and volume-weighted domain sizes according to the 'double-Voigt' method [17,18], which is equivalent to the Warren–Averbach approach [19].

In mechanically alloyed samples, due to different grain fracture mechanisms and oxygen inter-diffusion during the redox reaction, various stresses are expected to be induced during alloying and, consequently, the lattice microstrains for the observed crystalline phases should be significant. RMMS is defined as the amount (change in size or volume) by which a crystal lattice deforms under stress or force and is given as a ratio of the deformation to the initial size of the lattice.

The temperature evolution of lattice parameters, average grain size, regarded as the volume-weighted crystallographically coherent domain size, and RMSS, as obtained from the calculations using the integral breadth method are depicted in Figs. 3–5.

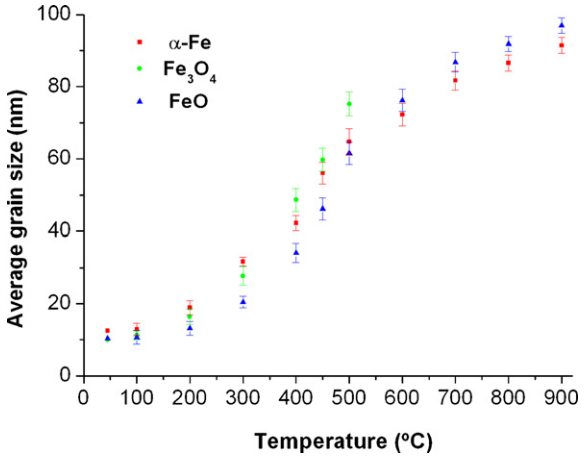

Fig. 4. Temperature evolution of average grain size of the identified phases.

The lattice parameter a calculated from the Bragg peaks positions determined from fitting of the whole XRD pattern (Fig. 3)

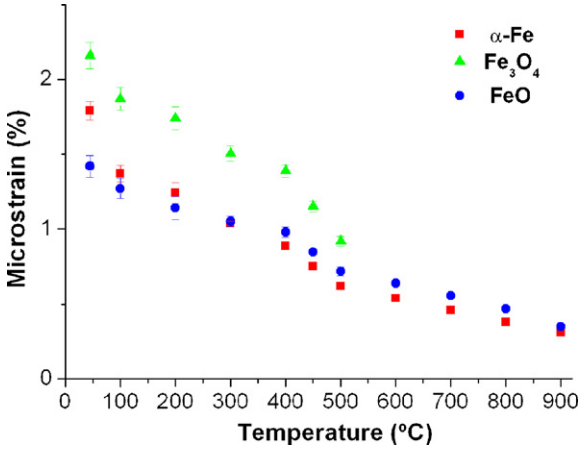

Fig. 5. Temperature evolution of lattice microstrains of the identified phases.

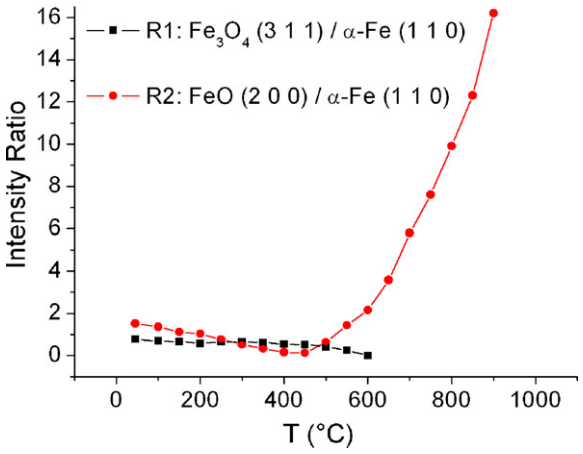

Fig. 6. Intensity ratios between main Bragg peaks of the Fe_3O_4 and α-Fe phases, and respectively between main Bragg peaks of the FeO and α-Fe phases at different temperatures, as revealed from the numerical fitting of the XRD patterns (Figs. 1 and 2). Line is for eye guiding only.

shows a continuous increase with temperature, due to the lattice expansion as a result of thermal effects. This is observable also in the synchrotron XRD patterns where the observed Bragg peaks shift continuously to higher reticular distances, with increasing temperature.

The average grain size depicted in Fig. 4 as a function of temperature, confirms the trend observed on XRD patterns regarding the continuous narrowing of the Bragg peaks with temperature. All the observed crystalline phases, α-Fe, Fe_3O_4 and FeO show similar trend, i.e. continuous increase of the average grain size, from about 10 nm at ambient temperature, up to around 90–95 nm for the pattern recorded at 900 °C. The increase is continuous, nevertheless there is a sharper increase between 400 °C and 500 °C, a range that corresponds roughly to the interval where the reversed reduction reaction takes place and FeO starts to form again, as observed in the XRD patterns.

Lattice microstrain calculated for all three phases is plotted as a function of temperature in Fig. 5. Contrary to the grain size evolution, the lattice microstrain decreases steadily with increasing temperature. As the crystallites grow with increasing temperature, the stresses induces in the grains during milling is reduced and the calculated microstrain is continuously reduced. Similar to Fig. 4, between 400 °C and 500 °C a sharper decrease of the microstrain is observed for all the phases. This range corresponds to the initiation of the reversed reduction reaction and formation of FeO.

The evolution of the phase structure with the temperature and the transformation occurring in the different stages of annealing may be followed by plotting the ratio between the main Bragg reflections of the constituent phases. In Fig. 6 we plot the intensity ratios R1 between Fe_3O_4 (3 1 1) and α-Fe (1 1 0) and R2 between FeO (2 0 0) and α-Fe (1 1 0) diffraction peaks, respectively. This approach constitutes only an estimation of the relative proportion of different phases, since it does not take into account the whole profile of all the diffraction peaks observed in the spectrum.

One can observe that, as it is also noticed in the diffraction pattern (Fig. 1), the wüstite is the predominant phase at 45 °C and then decreases slowly, its main Bragg line intensity reaching a minimum at 450 °C. After this temperature, the intensity of FeO increases very fast, and at about 900 °C, the iron Bragg line represents only 6% of the FeO main Bragg peak. This means that the formation of wüstite by reduction of Fe_3O_4 and the oxidation of the Fe is almost complete. This phase transformation is, as we already mentioned, irreversible, the sample quenched down to the ambient temperature presenting only the diffraction pattern of FeO.

It is possible from XRD measurements of crystalline samples to calculate the texture coefficient using the following formula [20]:

$$T_{hkl} = n\left(\frac{I_{hkl}}{I^0_{hkl}}\right)\sum_n \frac{I_{hkl}}{I^0_{hkl}} \quad (1)$$

T_{hkl} being the texture coefficient of the corresponding Bragg reflection, I_{hkl} its integral intensity as determined by numerical fitting of XRD patterns and $I^0{}_{hkl}$ corresponds to the theoretical Bragg peak intensity (from the ICDD file) and n is the number of Bragg peaks observed.

The texture results for the main Bragg peaks of α-Fe (1 1 0), FeO (2 0 0) and Fe_3O_4 (3 1 1) calculated using Eq. (1) show coefficients between 0.7 and 0.9 for all the XRD patterns. Therefore, results depicted in Fig. 6 must be cautiously taken into account, as it constitutes only an estimation of the amount ratios of different phases observed, as not the whole profile was considered for the calculations.

The strict control of the stoichiometry and the phase composition at every temperature stage is essential for the use of such mixed powders made of ferromagnetic and antiferromagnetic phases for magnetic applications, since they exhibit the exchange bias effect.

3.2. Isothermal annealed powders: structural properties

In order to confirm these findings, we have performed isothermal annealing of the as-milled powder at 250 °C, 400 °C, 550 °C and 720 °C for 1 h in high vacuum. The heating rate up to the annealing temperature was 2 K/min. The resulting powders were structurally characterized by means of SEM. Figs. 7 and 8 present selected SEM images of the samples as-milled and annealed at

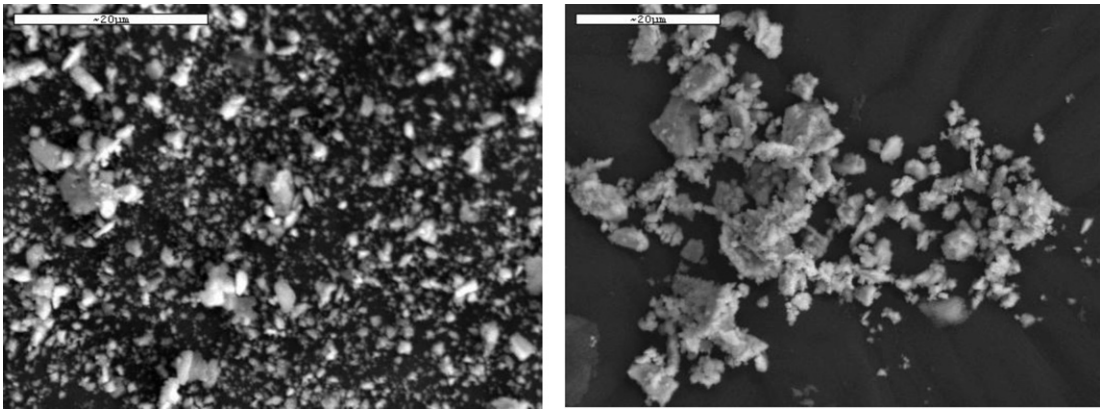

Fig. 7. SEM images of samples as-milled (left) and annealed at 200 °C (right).

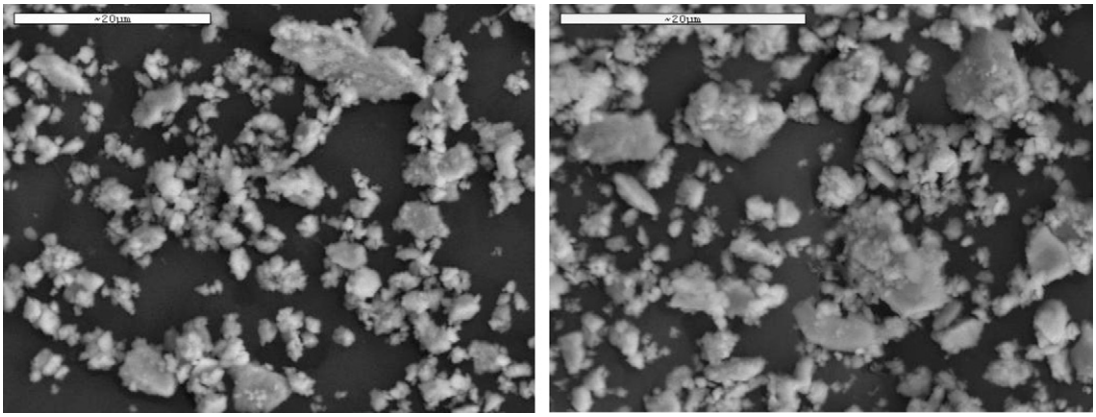

Fig. 8. SEM images of samples annealed at 400 °C (left) and 550 °C (right).

various temperatures. While as-milled sample shows a quasi-uniform structure with small and rather dispersed grains, with few large aggregates, the annealed samples present a structure with larger aggregates, resulted from coalescence of small grains during annealing. With increase of the annealing temperature, more aggregates are observed at the expenses of small, isolated grains.

3.3. Magnetic properties

Magnetic measurements have been performed in order to investigate the expected exchange bias effect but also to obtain important magnetic parameters such as the saturation magnetization, coercive field, etc. An important aspect is to correlate these parameters with the observed microstructure of the mixed nangranular powders and with the phase composition in various stages of annealing, as it has been revealed by the synchrotron X-ray diffraction study. To study the influence of the various phase compositions of the system in different stages of annealing, exerted onto the magnetic properties, such as the change in the magnitude or the sign of the exchange bias field, the hysteresis loops of the annealed at 250 °C and 400 °C samples have been performed and compared with the loops of the as-milled sample.

First, the samples were zero-field-cooled at 4.2 K and the hysteresis loop was recorded in fields up to 2.5 T. Then the sample was heated up to 280 K and the hysteresis loop was again recorded. In the last experiment, from the maximum value of 2.5 T the field was raised at 5 T and the sample was field-cooled with the 5 T field applied during the cooling. When the sample reached 4.2 K, the hysteresis loop was measured again. All the obtained hysteresis loops are plotted in Figs. 9–11.

Magnetic behaviour is similar in the case of the 3 samples: as-milled and annealed at 250 °C and 400 °C. Maximum specific magnetization is about 55 Am^2/kg, with a shape typical for soft FM/AF systems. The occurrence of the coercivity in such systems is due to the enhanced exchange coupling between FM and AF layers of atoms at the nanograins interfaces and/or grain boundaries.

We have also observed in the as-milled sample, at 4.2 K, a noticeable shift of the coercive field towards negative values, in other words, the occurrence of an exchange bias effect. The exchange bias field is calculated as:

$$H_e = (\left|H_c^-\right| - H_c^+) \quad (2)$$

where H_c^- and H_c^+ are the coercive fields recorded on descendent and ascendent loop branches, respectively.

The field cooling produces partial alignment of the magnetic domains. Thus, for temperatures below $T_{Néel}$ one observes slight increase of the magnetization and of the coercive field. It is also worth noticing that the exchange bias effect decreases with the

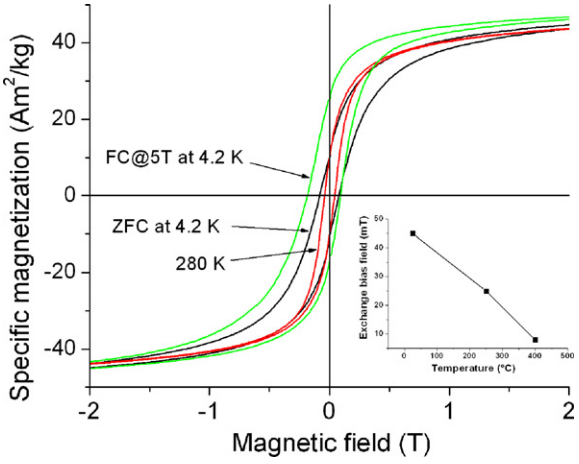

Fig. 9. Hysteresis loops for the as-milled sample: (a) ZFC at 4.2 K; (b) ZFC at 280 K and (c) FC@5 T at 4.2 K, magnified in the low applied field part. Inset: the exchange bias field measured as a function of the annealing temperature.

enhancement of the annealing temperature (as in the inset of Fig. 4) down to 6 mT for the sample annealed at 400 °C. This tendency is in agreement with the high amount of FeO observed in the phase composition in as-milled sample, while this relative proportion is diminished at higher temperatures due to the redox reaction (see Fig. 1), or for the annealed samples compared with the as-milled one.

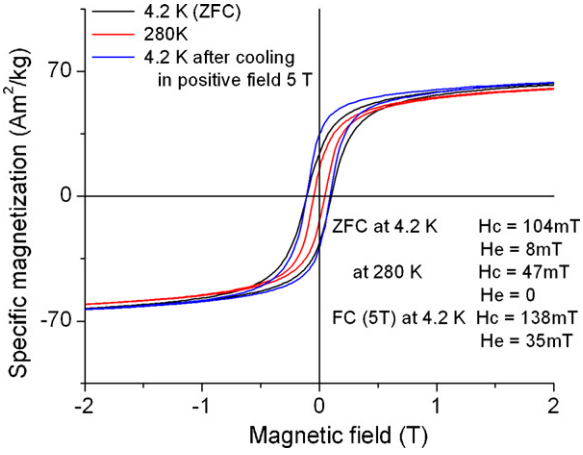

Fig. 10. Hysteresis loops for the sample annealed at 250 °C: (a) ZFC at 4.2 K; (b) ZFC at 280 K and (c) FC@5 T at 4.2 K, magnified in the low applied field part.

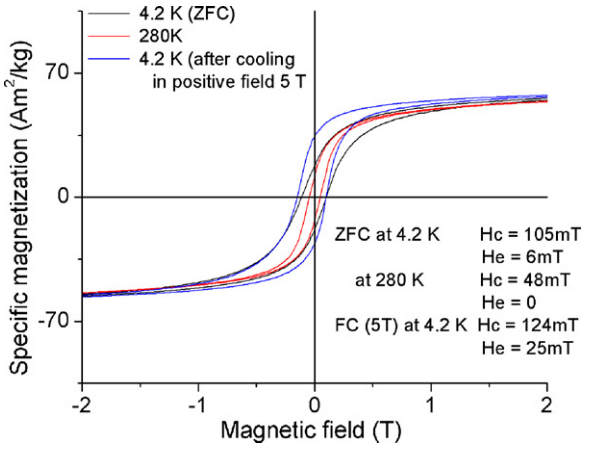

Fig. 11. Hysteresis loops for the sample annealed at 400 °C: (a) ZFC at 4.2 K; (b) ZFC at 280 K and (c) FC@5 T at 4.2 K, magnified in the low applied field part.

Besides the effect of the important amount of FeO in the phase composition of the samples, the decrease of the exchange bias effect is also related to the increased grain size (observed from XRD studies) and decrease of inter-grain distances (observed from SEM) after annealing the nanostructured powders. Nogués et al. [5] showed that in FM-AFM ball milled nanogranular powders, for a fixed FM/AFM ratio, the exchange bias (EB) effect is strongly affected by the evolution of the microstructure during milling and/or annealing. Both the grain size and the inter-grain distances, equivalent to AFM thickness in thin films, are influencing the EB effect. In our case the optimum EB effect is related to small grain size and phase microstructure in the as-milled sample, as increasing of the grain size and reduction of inter-grain distances obviously reduces this effect. Nevertheless, the correct quantification of these effects on the EB is difficult to perform [5]. It is also important to notice that correlations between the phase structure observed in synchrotron XRD at various temperatures and the magnetic data taken for samples after isothermal annealing should be considered only qualitatively since the annealing procedures, while comparable in terms of annealing temperatures and time, are slightly different regarding the heating rates.

4. Conclusions

The temperature evolution of the phase structure of a mixture of Fe and Fe_3O_4 (magnetite) powders, obtained by ball milling for 50 h at room temperature, has been studied by energy-dispersive in situ X-ray diffraction of synchrotron radiation. The nanocomposite powder is proven to undergo during preparation an incomplete redox reaction with formation of FeO. This reaction is favored due to the high energy developed during the milling and alloying. Two different stages of phase transformation are identified. In the first stage, between 45 °C and 450 °C, the FeO content decreases continuously in the sample and α-Fe and magnetite are the main phases identified in the XRD patterns. In the second stage, between 500 °C and 900 °C, the FeO phase starts to appear again in the detriment of the magnetite that completely disappear at around 600 °C. Magnetite and iron powders are gradually transformed via redox reaction and wüstite is the main phase observed in the sample at the end of this heating stage. A significant exchange bias effect related to FeO content and to an optimum of the microstructure (phase composition, small grain size, optimal inter-grain distances), is observed for as-milled sample, the effect being less pronounced upon annealing the nanograin powders.

Acknowledgements

The authors wish to acknowledge the help of Radu Nicula and Christian Lathe from MAX 80 beamline at HASYLAB during the XRD measurements. The financial support in the frame of the Marie Curie Host Development project HPMD-CT-2001-00089 as well as from Romanian Ministry of Education and Research via PN II project 12-129 is gratefully acknowledged.

References

[1] E. Bonetti, L. del Bianco, S. Signoretti, P. Tiberto, J. Appl. Phys. 89 (2001) 1806.
[2] L. del Bianco, D. Fiorani, A.M. Testa, E. Bonetti, L. Savini, S. Signoretti, Phys. Rev. B 66 (2002) 174418.
[3] L. del Bianco, D. Fiorani, A.M. Testa, E. Bonetti, L. Signorini, Phys. Rev. B 70 (2004) 052401.
[4] J. Nogués, I.K. Schuller, J. Magn. Magn. Mater. 192 (1999) 203–232.
[5] J. Nogués, J. Sort, V. Langlais, V. Skumryev, S. Suriñach, J.S. Muñoz, M.D. Baró, Phys. Rep. 422 (2005) 65–117.
[6] J. Ding, W.F. Miao, E. Pirault, R. Street, P.G. McCormick, Scripta Mater. 35 (1996) 1307.
[7] J. Ding, W.F. Miao, E. Pirault, R. Street, P.G. McCormick, J. Magn. Magn. Mater. 177–181 (1998) 933.
[8] B. Kämpfe, F. Luczak, B. Michel, Part. Part. Syst. Char. 22 (2006) 391–396.
[9] M. Seqqat, M. Nogues, O. Crisan, J. Magn. Magn. Mater. 157 (1996) 225–226.
[10] D. Predoi, O. Crisan, A. Jitianu, Thin Solid Films 515 (2007) 6319.
[11] O. Crisan, M. Angelakeris, N.K. Flevaris, J. Optoelectron. Adv. Mater. 5 (2003) 959–962.
[12] O. Crisan, J.M. Le Breton, G. Filoti, Sens. Actuators, A 106 (2003) 246.
[13] O. Crisan, Y. Labaye, L. Berger, J.M. Greneche, J.M.D. Coey, J. Appl. Phys. 91 (2002) 8727.
[14] O. Crisan, J.M. Greneche, J.M. Le Breton, Eur. Phys. J. B 34 (2003) 155.
[15] K. Syassen, Datlab, version 1.38XP MPI/FKF Stuttgart, Germany, 2005.
[16] H.P. Klug, L.E. Alexander, X-ray Diffraction Procedures, John Wiley, New York, 1974.
[17] D. Balzar, H. Ledbetter, J. Appl. Cryst. 26 (1993) 97.
[18] D. Balzar, J. Res. Nat. Inst. Stand. Technol. 98 (1993) 321.
[19] B.E. Warren, X-ray Diffraction, Addison Wesley, Reading, MA, 1969.
[20] D.N. Lee, J. Mater. Sci. 34 (1999) 2575.